Registration of 3D Medical Images using Simple Morphlogic Tools

J.B.A. Maintz,
P.A. van den Elsen,
and M.A. Viergever

UU-CS-1998-23
August 1998

ISSN: 0924-3275

Registration of 3D Medical Images using Simple Morphological Tools

J.B. Antoine Maintz, Petra A. van den Elsen, and Max A. Viergever

Image Sciences Institute, PO Box 85500, AZU-E.01.334, NL-3508 GA Utrecht, the Netherlands. Email: Twan.Maintz@cv.ruu.nl

Abstract. Multimodal medical images are often of too different a nature to be registered on the basis of the image grey values only. It is the purpose of this paper to construct operators that extract similar structures from these images that will enable registration by simple grey value based methods, such as maximization of cross-correlation. These operators can be constructed using only basic morphological tools such as erosion and dilation. Simple versions of these operators are easily implemented on any computer system. We will show that accurate registration of images of various modalities (MR, CT, SPECT and PET) can be obtained using this approach.

1 Introduction

Registration and hybrid visualization of 3D medical images has received ample attention from researchers in the past few years. The reasons for this may be clear: there are numerous applications in diagnostic as well as treatment settings, benefitting from integrating the complementary character of multimodal images. Notable application fields include neurosurgery and radiation therapy planning (Taylor, Lavallée, Burdea & Mösges 1996). For example, in the latter field, dose calculation is done best using a CT image, while often the target area can best be identified in an MR image. A second important reason is the recent availibility of computing power and computer architecture that can handle the entire bulk of 3D data –even though the size of clinical images has also grown considerably– while older methods often required data reduction of the images to, *e.g.*, a limited point set, surface, or abstract representation. Such computing power gives access to a class of so-called *voxel based* methods, which are preferable to previous methods in most cases.

Existing 3D rigid –*i.e.*, restricted to translational and rotational transformations– registration methods can be divided into extrinsic (external attachment based) and intrinsic (patient related) approaches (van den Elsen, Pol & Viergever 1993). Examples of extrinsic registration methods include methods based on fiducial markers (van den Elsen & Viergever 1994), a facial mould (Schad, Boesecke, Schlegel, Hartmann, Sturm, Strauss & Lorenz 1987) or a stereotactic frame (Vandermeulen 1991). Compared to these methods, voxel based methods (Woods, Maziotta & Cherry 1993, Hill, Studholme & Hawkes 1994, Maintz, van den Elsen & Viergever 1994, Maintz, van den Elsen & Viergever 1995, Studholme, Hill & Hawkes 1995, Viola & Wells III 1995, van den - Elsen, Maintz, Pol & Viergever 1995, Maintz, van den Elsen & Viergever 1996, Maes, Collignon, Vandermeulen, Marchal & Suetens 1996*a*, Maes, Collignon, Vandermeulen, Marchal & Suetens 1996*b*) are more patient friendly, and show higher reproducibility. Moreover, retrospective registration is now possible, as are extensions to non-rigid registration. Examples of intrinsic registration approaches other than voxel based methods are landmark registration (Evans, Marrett, Collins & Peters 1989, Hill, Hawkes, Crossman, Gleeson, Cox, Bracey, Strong & Graves 1991), surface based registration (Levin, Pelizzari, Chen, Chen & Cooper 1988, Pelizzari, Chen, Spelbring, Weichselbaum & Chen 1989), and hybrids of these techniques. Compared to these methods, voxel based

methods are better reproducible and less labour intensive. Voxel based methods are considered extremely promising with respect to accuracy (Viergever, Maintz, Stokking, van den Elsen & Zuiderveld 1995).

In this paper, we investigate the use of morphological operators for voxel based registration. Multimodal medical images are often of too different a nature to be registered directly on the basis of the image grey values only. It is the purpose of this paper to construct operators that extract similar structures from these images that will enable registration by maximization of the cross-correlation or a similar measure. The methods constructed are related to conventional surface based methods. However, instead of binary-valued surfaces we employ real-valued 'surfaceness' images obtained from the original images, thus employing more of the available image content. The operators involved can be constructed using only concatenations of basic image operations such as computing the maximum or minimum of a small region. We will show that accurate registration of images from various different modalities (MR, CT, SPECT and PET) can be obtained using this approach.

2 Methods

In the following section we will define the morphological operators featuring in our registration approach. The features extracted from the images by these operators can be used for registration by optimizing the cross-correlation value. Section 2.2 details the cross-correlation maximization algorithm. The next sections describe the morphological operator compounds that can be employed in three specific applications: CT-MR registration (2.3), MR-SPECT registration (2.4), and MR-PET registration (2.5). The final section (2.6) describes verification methods for the registrations obtained. Registration results of the developed methods will be shown in section 3.

2.1 Morphological operations

The operators used in this paper stem from the field of mathematical morphology (Serra 1982, Haralick, Sternberg & Zhuang 1987, Serra 1988); all are well known and frequently used there. They are simple in the sense that they usually have an intuitive geometrical interpretation, and that they allow straightforward implementations on a computer platform, although fast and elegant approaches require quite some sophistication.

The *erosion* ε of a function $f(x)$ by a symmetrical planar structuring element B is defined as $\varepsilon(f)(x) = \inf_{b \in B}(f(x-b))$. The dual operation of erosion is called *dilation* (δ), which is defined by $\delta(f)(x) = \sup_{b \in B}(f(x-b))$. The effects of the erosion and dilation operations are usually intuitively clear: erosion will "eat away", abrade the boundary of objects, whereas dilation will expand objects at the boundary.

Erosion and dilation are dual operations, *i.e.*, erosion of $f(x)$ equals dilation of the complement of $f(x)$. They are not inverses, owing to the non-linear character of the operations; there are multiple input images that produce the same result when eroded. The smallest pseudo-inverse, *i.e.*, the composition of erosion and dilation, has some interesting properties. The morphological *opening* γ is defined as the composition of erosion and dilation, the morphological *closing* φ is defined as the composition of dilation and erosion: $\gamma = \delta\varepsilon$ and $\varphi = \varepsilon\delta$. Their effects are again intuitively clear: a closing removes holes and thin cavities, and an opening opens up holes that are near (with respect to the size of the structuring element) a boundary, and removes small object protuberances. An example is given in figure 1.

Since the erosion and dilation operations act most prominently on object boundaries, the *differences* between the eroded, the dilated and the original images bring out edge information of the original. The *morphological gradient* g is defined as the difference between a dilated and an eroded image: $g(f) = \delta(f) - \varepsilon(f)$. This 'thick' gradient

Fig. 1. Example of opening (middle) and closing (right) by a square structuring element on a grey valued MR image (left).

can be decomposed into two 'half' gradients: an 'inner' gradient $g^- = f - \varepsilon(f)$ adhering to the inside of objects, *i.e.*, to the bright side of the edge, and an outer gradient $g^+ = \delta(f) - f$.

The ideas of erosion and dilation can also be employed for contrast enhancement and deblurring of grey valued images. The contrast can be enhanced by replacing each pixel value by either the dilated or eroded value, whichever one was closer to the original value:

$$f_{\text{enh}} = \begin{cases} \delta(f) & \delta(f) - f \leq f - \varepsilon(f) \\ \varepsilon(f) & \text{otherwise.} \end{cases}$$

This technique can be shown to exactly reconstruct a convex homogeneous object that has been blurred by Gaussian convolution. This result does not hold in the general case, but nonetheless pleasing results can be obtained, as figure 2 shows. Upon iterating the deblurring operation, it always converges to a stable result (Kramer & Bruckner 1975).

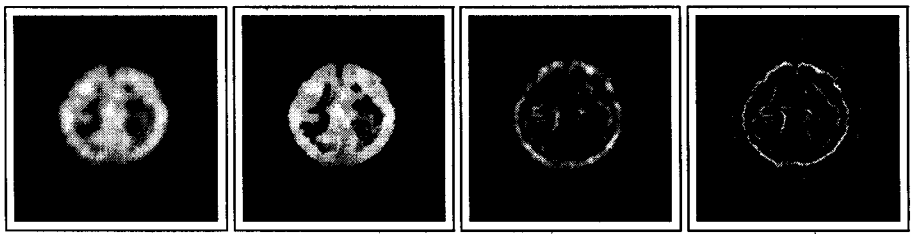

Fig. 2. Example of deblurring applied to a SPECT image. From left to right: the original 128×128 SPECT image, the image after a single step of deblurring with a 3×3 square, the inner gradient of the original, and the inner gradient of the deblurred version.

It is often desirable to remove small objects from images, while keeping larger objects completely intact. The standard opening does not have the right properties to do this, because the shape of objects is not completely preserved. An approach to remedy this is to use *opening by reconstruction*. Before defining this, we need the concept of *geodesic dilation* $\delta_g = \min(\delta(f), g)$, where g is a 'control' image: f is dilated in the usual way, but constrained so as to never grow 'outside' of the control image g.

If the geodesic dilation is iterated until stability is reached, it is called *reconstruction by dilation*. The opening by reconstruction, finally, is the composition of erosion, and reconstruction by dilation. Here, the erosion removes small and thin objects, and the following reconstruction by dilation brings the remaining objects back to their original form. An example can be seen in figure 3.

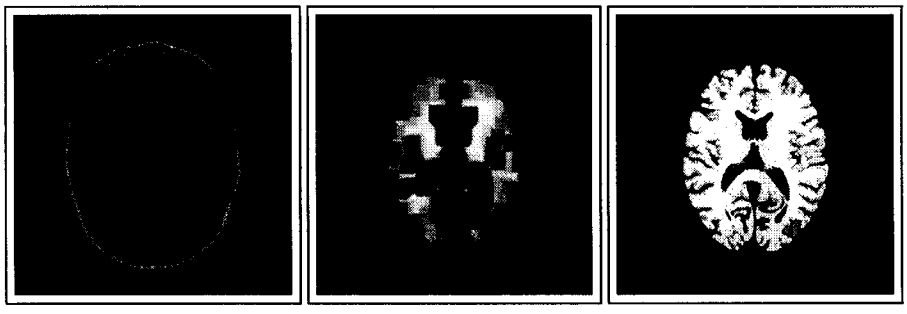

Fig. 3. Example of opening by reconstruction of an MR image. Left: original image. Middle: eroded image. Right: final image, after reconstruction and subsequent thresholding. The original image is used as the control image in the reconstruction.

2.2 Registration method

Our aim is to use the morphological operators described in the previous section to extract feature images from multimodal images that show enough similarity as to allow for rigid registration by maximizing the cross-correlation value.

An exhaustive search of the 6-dimensional parameter space (three translations, three rotations), is not a realistic option because of the high computational complexity. We chose a *hierarchical* multi-resolution approach to handle this optimization problem. From each of the feature images to be registered a multi-resolution pyramid is created. The bottom layer of each pyramid equals the original image, and a number of layers are created by repeated downsampling by a factor of two in each dimension. Three (SPECT/PET) to five (high resolution CT) layers are created. In the top layer an exhaustive search of the parameter space is now feasible. We use the term 'exhaustive' loosely here, as we restrict the parameter space to realistic transformations. The global optimum found in the search, as well as local optima within a certain percentage of the global one are retained, and used as search seeds in the next pyramid layer. The search spaces in adjacent layers are narrowly tuned lest to miss a local optimum.

2.3 Application: CT and MR registration

Direct use of the morphological (inner) gradient often causes misregistration when the cross-correlation is optimized in the above described way, especially where images with a large slice thickness are concerned. The reason for this is that various edges, notably the skull and skin edges, are frequently very close together, which causes the wrong edges to be aligned by the registration algorithm. We therefore extended the method to only use the skin edge. To detect this edge using a morphological inner gradient, we first need to remove all internal structures in the images, so the inner gradient acts upon an image containing only the skin edge. These internal structures can be removed by

applying a closing for the removal of dark structures followed by an opening for the removal of bright structures. In the case of MRI, the nature of the images is such that the opening is not even necessary. The only parameters that need to be established are the sizes of the structuring elements used, which should be large enough to obtain the desired effect, while kept sufficiently small to minimize distortion effects. The operations actually used can be found in table 1. As the table shows, a different approach is used for MR T1 and T2 weighted images, which is necessitated by the completely different nature of the images. With poor quality initial images, both the CT and MR final edgeness images can still be improved (*i.e.* made more homogeneous) by applying a threshold. The actual threshold value does not appear to be critical, and we fixed it to 20% of the image maximum after processing. Figure 4 shows examples of the final feature images.

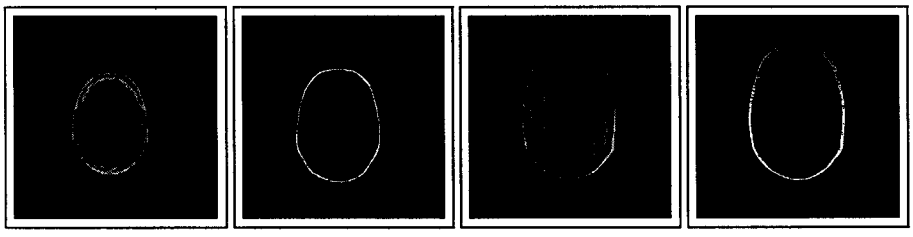

Fig. 4. Examples of the original and edgeness feature images used in CT (left two images) to MR (right two images) registration.

It may seem –when looking at the final feature images– that the method reduces to surface based registration. The feature images, however, are not nearly binary, but have an extensive grey range, nor are the depicted structures thin. These very properties ensure proper convergence of the registration method.

2.4 Application: SPECT to MR-T1 registration

With SPECT[1] to MR-T1 registration, we use the same approach as with CT to MR registration: to avoid the risk of misregistration, *i.e.,* the alignment of anatomically non-corresponding edges upon using simple edgeness images, we use a morphological operator to select the skin edge from the MR. The edgeness is then computed both from MR and SPECT by applying a morphological inner gradient. The SPECT edgeness image can be improved upon by using morphological deblurring as a preprocessing step. Examples of the SPECT feature images can be seen in figure 2 and of the MR feature image in figure 4.

2.5 Application: PET to MR registration

Registration of PET[2] to MR-T1 images based on the skin edge is not feasible, since the skin edge cannot be seen in a PET image like in a SPECT image. Our PET/MR registration is therefore based on the cortex edge, rather than the skin edge as with SPECT/MR registration.

[1] In this application we use ^{99m}Tc-HMPAO perfusion SPECT images.

[2] In this application we use FDG (fluorodeoxyglucose) or ethyl 8-fluoro-5,6-dihydro-5-methyl-6-oxo- H-imidazo [1,5-α]-[1,4] benzodiazepine-3-carboxylate (Flumazenil) PET images.

The extraction of the cortex edge from the PET image is relatively easy, since it is the dominant edge of the image. We improve the inner gradient image in much the same way as before (cf. CT to MR registration) by removing internal structures with a closing and an opening. In addition, since PET images are somewhat more blurry than MR images, we sharpen the image by a deblurring operation.

In the MR image, we suppress the skin edge, and endeavor to 'select' only the cortex edge. We can achieve this by removing all structure outside of the cortex in the MR image, by applying an opening to it. This can either be a plain opening or an opening by reconstruction. While the latter produces less artefacts, it is also more time consuming to perform. The disadvantage of using an opening is that the cortex and the structures outside of it need to be well separated in order for the opening to create the desired result. Although this condition is met for transverse image slices above the eyes, it breaks down for slices near the base of the brain. A solution to this is to simply stop the reconstruction process after a number of iterations, instead of iterating until stability. Because the 'seed' of the reconstruction process is an eroded version of the original image (see figure 3), the first iterations will reconstruct the cortex, and only further iterations will allow the skin and other structures to 'grow back'. Since the size of the applied erosion is known, the number of iterations after which to stop the reconstruction is easily estimated.

The proposed PET feature images for registration can be seen in figure 5, and the MR feature images before computing the inner gradient in the figures 1 and 3.

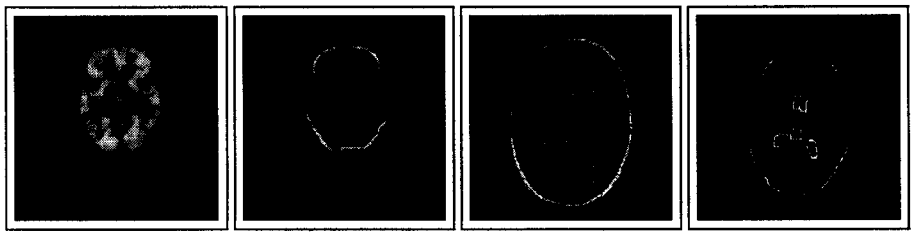

Fig. 5. Example of PET and MR feature images as used in PET to MR registration. The left two images show an original PET slice and the corresponding slice from the feature volume, and the right two images show an original and feature MR slice.

For PET to MR-T2 registration, the above described method for PET to MR-T1 registration can be used. However, since the cortex edge is much brighter in T2 weighted images than in T1 weighted MR images, we can suffice with a simpler feature extracting scheme for the MR image: an opening followed by a threshold and an inner gradient.

2.6 Accuracy verification of the registration

In this paper, we use the methods of visual inspection and comparison to registration based on fiducial skin markers in all of the applications. The visual inspection was performed by segmenting meaningful contours from a slice of one image, and overlaying them onto a corresponding slice from a registered image. This procedure is carried out using around four transversal slices, as well as the midsagittal and midcoronal slice from the MR image involved. The 'fit' of the contours is then assessed visually. In the case of CT to MR registration, we additionally used a cadaver study for validation, and also compared the registration results to those obtained by an earlier method: L_w *correlation*, a method which is based on optimizing the cross-correlation of edgeness images extracted from the original images involved by means of convolution with

From \ To	MR-T1	MR-T2
CT	CT: close(4), open(8), inner grad.	CT: close(4), open(8), inner grad.
	MR: close(4), inner grad.	MR: open(1), threshold(low), close(2), inner grad.
SPECT	SPECT: deblur, inner grad.	
	MR: close(4), inner grad.	
PET	PET: deblur, close(3), open(3), inner grad.	PET: deblur, close(3), open(3), inner grad.
	MR: open by reconstruction, inner grad.	MR: open(4), threshold(low), inner grad.

Table 1. Summary of morphological registration methods. Bracketed numbers indicate the structuring element half size used (in millimeters). Only square structuring elements were used.

Gaussian derivatives, see (Maintz, van den Elsen & Viergever 1997). Since this method was designed specifically for CT to MR registration, it could not be used to verify the registrations involving SPECT or PET. Finally, with PET to MR registration and CT to MR registration, 9 patients were implanted with four fixed markers, which were used to establish a comparative registration (West et al. 1996). The verification methods used are summarized in table 2.

	visual inspection	skin markers	fixed markers	comparison to L_w correlation	cadaver study
CT/MR	✓	✓	✓	✓	✓
PET/MR	✓	✓	✓	**np**	**np**
SPECT/MR	✓	✓	–	**np**	**np**

Table 2. Summary of verification methods used. Legend: ✓: method used, –: method not used, **np**: use of the method is not possible.

3 Results

3.1 Application: CT to MR registration

Studies validated by fiducial skin markers and L_w correlation The patients involved in these studies were supplied with three markers glued to the skin just before image acquisition (van den Elsen, Viergever, van Huffelen, van der Meij & Wieneke 1991, van den Elsen & Viergever 1994). The markers are attached near the temporomandibular joints and at the nasion. The marked points can be located with subslice accuracy using near-automatic —two user-identified seed points are required for each marker— methods in each of the images involved. The marker based registration is then performed by aligning (in the least squares sense) the three points located in each of the images involved.

In previous work (Maintz et al. 1995, Maintz et al. 1997), we examined the use of edgeness images –as generated from CT and MR volumes by means of computing a scaled gradient magnitude– for registration purposes. The edgeness computing operator, called L_w, appeared well suited for the task of CT to MR registration.

The two studies involved[3] were registered by means of the new morphologically based method, as well the above mentioned skin marker and L_w based methods. As a measure for the difference between the various registration results, we use the *maximum* and *mean* distance between two corresponding voxels as transformed by the different registration results. We compute these distances taking into account all voxels within a sphere containing the entire head, so these measures are in fact overstimates of the 'true' error, *i.e.* the error based only on patient related voxels. Table 3 shows the maximum and mean distances between all of the registrations. Please note that these distances are not error measures, as the registration used for reference will also contain a certain error. The results of the visual inspection was that shifting the registered contours did not improve the morphologically based registration, and that in a number of image areas there is a clear preference for the morphologically based match over the marker based registration.

	Study 1			Study 2		
		Morph.	L_w		Morph.	L_w
Maximum distance	Marker	6.8	3.3	Marker	4.2	6.0
	Morph.		4.3	Morph.		5.8
		Morph.	L_w		Morph.	L_w
Mean distance	Marker	3.9	1.9	Marker	2.8	3.4
	Morph.		2.6	Morph.		3.3

Table 3. Maximum and mean distances (in millimeters) between CT to MR registrations as obtained by marker based, L_w based, and morphologically based registrations.

Studies validated by fixed fiducial markers The patient group involved here comprises seven patients, each implanted with four fixed fiducial markers, any trace of which was removed from the images before feature detection was applied. The reference registration was computed based on the fiducials. The validation of our morphologically based registration was done in a more elaborate way than in the previous study, namely by computing the maximum and median distance between the two registrations in ten small anatomically relevant volumes of interest, which were located in the MR image by clinical experts[4]. Per patient, six registrations were performed: the CT was registered to a proton density (PD) weighted MR image, a T1 weighted MR image, a T2 weighted MR image, and geometrically rectified (Chang & Fitzpatrick 1992) versions[5] of all of

[3] Study **I** contained a 256 matrix, 200-slice transversal T1-weighted FFE sequence MR image, with voxel dimensions of $0.98 \times 0.98 \times 1.0mm$, obtained on a 1.5 T Philips Gyroscan S15, and a 256 matrix, 100-slice transversal CT image, with voxel dimensions $0.94 \times 0.94 \times 1.55mm$, obtained on a Philips Tomoscan 350. Study **II** contained a 256 matrix, 100-slice transversal T1-weighted FFE sequence MR image, with voxel dimensions $0.9 \times 0.9 \times 1.55mm$, obtained on a Philips Gyroscan T5, and a 256 matrix, 128-slice transversal CT image, with voxel dimensions $0.7 \times 0.7 \times 1.5mm$, obtained on a philips Tomoscan LX. These images are –in terms of image quality– at the high end of current clinical practice.

[4] The method of computing the maximum distance differs from the one used in the previous study, since this particular validation study was part of an off-site blinded registration validation protocol. This is also the reason why median distances are used in this validation study instead of mean distances.

[5] Except for patient 6, MR T1.

the MR images[6]. An advantage of this patient group is that the fixed markers are most likely more reliable than the skin markers used in the previous section. The image quality in this group is considerably poorer, but not unrealistically so with respect to today's clinical practice. The results can be viewed in table 4. Note that, in this particular study, the geometrical rectification of the MR sets did not significantly alter the registration results.

The results of the visual inspection were less good than in the previous section. Although the actual inspection is made more difficult by the relatively poor quality of the images and the thicker slices, it is obvious that, at least for a number of patients, the morphologically based registrations could be improved.

	Maximum distances							Median distances						
Study #	1	2	3	4	5	6	7	1	2	3	4	5	6	7
CT-MR(PD)	4.7	11.0	19.0	6.8	8.2	9.9	4.7	4.0	5.5	8.9	2.7	4.0	4.5	3.7
CT-MR(T1)	7.4	12.8	8.4	9.1	9.1	10.5	4.0	5.6	7.0	7.6	8.4	4.7	4.8	3.6
CT-MR(T2)	4.2	3.4	6.1	5.1	6.0	6.3	5.0	3.4	3.2	5.3	4.8	4.6	4.0	4.4
CT-MR(PD rect)	1.4	9.9	7.3	9.0	7.4	6.4	1.4	1.2	6.7	6.9	7.2	3.0	3.2	0.8
CT-MR(T1 rect)	5.2	10.5	7.5	14.2	8.6	-	1.7	4.6	6.7	6.9	11.7	4.2	-	1.1
CT-MR(T2 rect)	4.9	6.5	5.4	3.4	3.7	6.2	4.4	4.5	5.3	4.6	3.2	3.0	5.1	3.8

Table 4. Maximum and median distances (in millimeters) computed over 10 anatomically relevant volumes of interest, between our morphologically based registrations and a reference registration based on fixed fiducials. The dash indicates the rectified MR volume was not available.

Study validated by a cadaver study One cadaver study[7] was included in the validation experiments. Cadaver based validation has several attractive properties: The images are free of motion artefacts, there is no need to pay heed to radiation dose with the CT acquisition, *i.e.*, the field-of-view can be chosen arbitrarily large, and external and internal markers can be attached and inserted without paying much attention to possible tissue damage. On the other hand, post-mortem changes in the anatomy could possibly make the data unrealistic.

The reference registration (Hemler, van den Elsen, Sumanaweera, Napel, Drace & Adler 1995) was obtained by inserting four glass hollow rods ($1.5/3.0mm$ inside/outside diameter) into the head of a human cadaver at different angles. These tubes were filled with a contrast agent, and detected in each of the modalities. The center lines of the detected tubes were used to compute the maximum and mean distances. Before applying the morphologically based registration method, the tube structures were eliminated from the images.

Since the contained (scanned) volume of the head in the CT image is of a size seldom encountered in clinical practice, these data provide us with an opportunity to simulate more clinically relevant registration cases by selecting an appropriate volume from the CT image, while keeping the reference registration based on the entire scanned volume. Also, from the original volumes images with thicker slices were simulated. The

[6] The CT images were 512 matrix, approximately 30 tranversal slices, with voxel dimensions $0.65 \times 0.65 \times 4.0mm$, obtained on a Siemens Dr-H. The MR (PD, T1 and T2-weighted) images were 256 matrix, approximately 23 transversal slices, SE sequence, with voxel dimension $1.25 \times 1.25 \times 4.0mm$, obtained on a 1.5T Siemens SP.

[7] The CT image was a 512 matrix, 180-slice transversal image, with voxel dimensions of $0.67 \times 0.67 \times 1.0mm$, obtained on a GE HiSpeed Advantage Helical CT. The MR image was a 256 matrix, 124-slice transversal 3D GRASS sequence image, with voxel dimensions $1.09 \times 1.09 \times 1mm$, obtained on a GE Signa 1.5T.

morphologically based registration was applied to all of the original and simulated volumes separately, and the registration results were compared to the reference registration based on the entire high-resolution volumes. The maximum and mean distances are given in table 5. The visual inspection showed that the registrations were accurate, with the exception of the registration using only the lower part of the CT volume. In the latter case an error in the order of a few pixels could be observed in some image areas.

Images used	Maximum distance	Mean distance
original volumes	1.1	0.4
$3mm$ slices	2.5	1.0
$5mm$ slices	3.7	2.1
lower CT volume only	4.6	2.2
upper CT volume only	2.1	0.7

Table 5. The maximum and mean distances (in millimeters) between the morphologically based registrations and the reference registration of a cadaver study.

3.2 Application: SPECT and MR registration

In this application, ^{99m}Tc-HMPAO SPECT images were registered to T1-weighted MR images[8]. The patient group comprised five patients, and the reference registration was provided by means of fiducial skin markers. Initially, the patient group was much larger, but, owing to the cumbersome nature in terms of image acquisition –the group consisted of children with tics and concentrative disorders– only in five cases could the markers be used successfully. This in itself is already an argument in favor of retrospective registration techniques. The maximum and mean distances between the marker based (reference) registration and the morphologically based registration of the five remaining patients are listed and table 6. The visual inspection gives the impression of imprecise

	Study #				
	1	2	3	4	5
Maximum distance	15.6	7.8	6.2	12.6	10.9
Mean distance	8.3	3.9	3.0	6.5	8.5

Table 6. The maximum and mean distances (in millimeters) between the marker based (reference) registration and the morphologically based registrations of five SPECT to MR registrations.

results when viewing most of the marker based registrations. Two of the morphologically based registrations could also be improved upon. The inaccuracy is also reflected in the relatively large errors in the table. We suspect the sometimes severe motion artefacts in the images to hamper proper registrations.

We can as yet not draw definite conclusions regarding the quality of the morphologically based registration, because of the poor quality of the images used, and the lack of precision in the marker based reference registation. More images need to be acquired for proper tuning and verification of the morphologically based registration method.

[8] The MR images were 256 matrix, 127 slice, FFE sequence T1-weighted transversal images, with voxel dimensions $0.78 \times 0.78 \times 1.25mm$, obtained on a Philips Gyroscan T5. The SPECT images were 64 matrix, with approximately 50 slices, ^{99m}Tc-HMPAO transversal images, with voxel dimensions $3.91 \times 3.91 \times 3.56mm$, obtained on a Picker PRISM 3000.

3.3 Application: PET to MR registration

Within this application, we used two types of validation: fixed implanted fiducial markers, and skin fiducial markers. In both cases visual inspection was also applied. The verification is the same as in the case of the CT to MR registration application: with the fixed markers, the median and maximum distances in ten anatomically relevant volumes of interest are computed, whereas with the skin markers the maximum and mean distances in a sphere containing the entire head are computed.

Studies validated by fixed fiducial markers Seven patient studies were used in these experiments (of which five concern patients also used in the CT to MR registration as validated by fixed fiducials). Of each patient, three MR studies and a PET study were acquired[9]. Of five patients the MR studies were also geometrically corrected (Chang & Fitzpatrick 1992). The registration results can be seen in table 7. Visual inspection is hard compared to CT to MR inspection, owing to the relatively poor image quality. The accuracy as assessed from visual inspection correlates well in a qualitative sense with the differences listed in table 7.

	Maximum distances							Median distances						
Study #	1	2	3	4	5	6	7	1	2	3	4	5	6	7
PET-MR(PD)	8.0	7.7	8.1	5.6	7.6	9.8	7.5	3.6	4.9	3.6	3.4	4.9	6.4	5.8
PET-MR(T1)	5.5	10.6	3.8	3.9	5.9	5.1	4.0	2.6	8.6	2.3	2.5	4.8	3.7	3.3
PET-MR(T2)	7.2	12.7	6.4	15.0	4.0	13.1	8.8	3.7	6.3	3.2	11.6	2.3	8.1	5.4
PET-MR(PD rect)	5.4	6.9	5.2	6.6	9.2	-	-	3.6	6.6	3.6	4.3	5.9	-	-
PET-MR(T1 rect)	6.2	4.4	4.5	-	7.7	-	-	4.5	3.2	3.7	-	5.1	-	-
PET-MR(T2 rect)	5.4	9.0	4.1	10.9	3.6	-	-	3.9	7.7	3.4	10.6	2.2	-	-

Table 7. Maximum and Median distances (in millimeters) computed over 10 anatomically relevant volumes of interest, between our morphologically based registrations and a reference registration based on fixed fiducials. If there is a dash in the table, the rectified MR volume was not available.

Studies validated by skin fiducial markers Four patient studies were involved in these experiments. Of three patients MR T1 weighted, MR T2 weighted, PET FDG, and PET Flumazenil images[10] were made. Of the fourth patient only an MR T1 weighted and a PET FDG study was made. For various logistic reasons, notably the short half life of the ^{11}C based Flumazenil, no markers were used in the Flumazenil studies. The markers in one of the FDG studies could not be detected properly because the used (clinically defined) field-of-view did not allow for proper inclusion of one of the markers. The remaining maximum and mean distances between the marker based registrations and the morphologically based registrations are listed in table 8. The visual

[9] The MR images were respectively PD, T1 and T2-weighted transversal SE sequence images, with a 256 matrix, containing approximately 23 slices, with voxel dimension $1.25 \times 1.25 \times 4.0mm$, obtained on a 1.5T Siemens SP. The PET image was a 128 matrix, 15 slice transversal FDG (^{18}F-fluorodeoxyglucose) image with voxel dimensions $2.59 \times 2.59 \times 8.0mm$, obtained on a Siemens/CTI ECAT 933/08-16.

[10] The T1 weighted MR images were 256 matrix, 127 slice FFE sequence images, with voxel dimensions $0.98 \times 0.98 \times 1.2mm$. The T2 weighted images were 256 matrix, 130 slice TSE sequence images, with voxel dimensions equal to the T1 weighted image. Both MR images were obtained on a Philips Gyroscan T5. The PET images, both Flumazenil and FDG studies, were 128 matrix, 31 slice images with voxel dimensions $2.35 \times 2.35 \times 3.38mm$, obtained on a Siemens/CTI ECAT 951/31R.

	Maximum distances				Minimum distances			
Study #	1	2	3	4	1	2	3	4
FDG-T1	-	7.5	4.6	8.8	-	5.1	2.4	6.6
FDG-T2	-	11.7	13.8	-	-	8.9	11.0	-

Table 8. The maximum and mean distances (in millimeters) between the marker based and morphologically based registrations of the FDG and MR studies involved.

inspection reveals that accurate marker detection is limited by the blurry nature of the PET images. Marker based alignment is therefore not the best of standards for PET to MR registration. The morphologically based registrations appear accurate in most cases, but in some cases a visible mismatch can be perceived when viewing the midsagittal plane. There seems to be no difference between the quality of registrations involving FDG PET images and the ones using Flumazenil PET images. The registrations involving T1 weighted MR images appear more accurate than the ones using T2 weighted MR images.

4 Discussion

We have applied the morphologically based registration techniques on many more image pairs than addressed in this paper. The ones reported here are those pairs that come with a reference registration that can be used for at least some validative measure. The methods perform satisfactorily in all cases of CT to MR registration with images of regular clinical protocols (although results are better when high resolution data is used), but –as the above sections showed– mismatches may still occur when functional images are involved. Generally, significant misregistrations can easily be perceived when inspecting the registration visually. It is not difficult to adapt the feature extraction procedure in these cases such that a satisfactory match is obtained. However, such interventions destroy the automatic nature of the whole registration process. As can be learned from West *et al.* (1996), our MR to PET registration accuracy measurements are comparable to most other registration algorithms, even though many methods in this study use manual intervention to optimize the registration.

In conclusion, simple morphological tools are capable of registering CT and MR images accurately and robustly, and provide acceptable PET to MR and SPECT to MR registrations in most cases. We have not found a simple procedure that adequately registers SPECT or PET with MRI in all cases considered; the variability in the data is too large to enable a fully robust registration paradigm.

A point we want to emphasize is that the reference registrations should not be regarded as a gold standard, *i.e.*, the distances in the tables should not be interpreted as errors. Such distances are at best *indicative* of the quality of the morphological registrations. In a number of cases, especially in the CT to MR application, it was clear from visual inspection that the morphologically based registration was of superior quality. Moreover, even with high resolution volumes (voxel volume $1mm^3$), experts sometimes could not distinguish between the quality of two matches, although the maximum distance between them exceeded $3mm$. This can have a number of causes, amongst which are local image distortion, the fact that the distance overestimates the 'true' error, the *rigid* transformation paradigm, the fact that a registration algorithm will perform better in those image areas dominant in the feature images (*i.e.*, at the edges used in the registration), *etc.*

In the opinion of these authors, voxel based registration methods will eventually outperform others. We are currently experimenting with mutual information based methods as developed by Collignon and co-workers (Collignon, Maes, Delaere, Vandermeulen,

Suetens & Marchal 1995), which produces visually attractive results on *almost all* of the image pairs used in this paper. However, these methods are as yet unsuitable for registration tasks that are severely time-constrained (such as intra-operative registration) or tasks that do not allow registration by means of a rigid transformation only (*e.g.* involving abdominal scans). Speed of the registration method is heavily dependant on the information content of the images involved. In this paper, by applying morphological operators, we have dramatically reduced the total information content of images, while simultaneously extracting feature information of corresponding anatomical structures. Also, we have shown that multi-resolution approaches can be used in the maximization procedure. Preliminary experiments corraborate that both the multi-resolution approach and the information reduction could be incorporated into mutual information based registration.

5 Acknowledgments

This research was supported in part by the industrial companies Philips Medical Systems, KEMA, Shell Industrial Exploration and Production, and ADAC Europe, as well as by the Netherlands ministries of Education & Science and Economic Affairs through a SPIN grant, and by the Netherlands Organization for Scientific Research (NWO), through a travel grant. Dr Paul Hemler and Dr Thilaka Sumanaweera are kindly acknowledged for their work on the cadaver study. Dr Jan Buitelaar and Alice van Dongen, MA are greatfully acknowledged for their assistance with the SPECT images. The images with implanted fixed markers used in the validation of the CT/MR and PET/MR registrations were acquired as part of the project "Evaluation of Retrospective Image Registration", NIH R01MS/CA 3392 6-01, coordinated by Dr Michael Fitzpatrick, Vanderbilt University. We are indebted to Jay West and Dr Michael Fitzpatrick for their help regarding these images. We also wish to thank Dr René Debets, Dr B. Sadzot and Christian Degueldre for their assistance in acquiring the PET images, and Dr Linda Meiners for helping out with the related MR protocol.

References

Chang, H. & Fitzpatrick, J. M. (1992), 'A technique for accurate magnetic resonance imaging in the presence of field inhomogeneities', *IEEE Transactions on medical imaging* **11**, 319–329.

Collignon, A., Maes, F., Delaere, D., Vandermeulen, D., Suetens, P. & Marchal, G. (1995), Automated multimodality image registration using information theory, *in* Y. Bizais & C. Barillot, eds, 'Information Processing in Medical Imaging', Kluwer Academic Publishers, Dordrecht, pp. 263–274.

Evans, A. C., Marrett, S., Collins, L. & Peters, T. M. (1989), Anatomical-functional correlative analysis of the human brain using three dimensional imaging systems, *in* R. Schneider, S. Dwyer III & R. Jost, eds, 'Medical imaging: image processing', Vol. 1092, SPIE press, Bellingham, WA, pp. 264–274.

Haralick, R. M., Sternberg, S. R. & Zhuang, X. (1987), 'Image analysis using mathematical morphology', *IEEE transactions on pattern analysis and machine intelligence* **9**(4), 532–550.

Hemler, P. F., van den Elsen, P. A., Sumanaweera, T. S., Napel, S., Drace, J. & Adler, J. R. (1995), A quantitative comparison of residual error for three different multimodality registration techniques, *in* Y. Bizais, C. Barillot & R. di Paola, eds, 'Information processing in medical imaging', Kluwer, pp. 389–390.

Hill, D. L. G., Hawkes, D. J., Crossman, J. E., Gleeson, M. J., Cox, T. C. S., Bracey, E. C. M. L., Strong, A. J. & Graves, P. (1991), 'Registration of MR and CT images for skull base surgery using pointlike anatomical features', *British journal of radiology* **64**(767), 1030–1035.

Hill, D. L. G., Studholme, C. & Hawkes, D. J. (1994), Voxel similarity measures for automated image registration, *in* R. Robb, ed., 'Visualization in biomedical computing', Vol. 2359, SPIE Press, Bellingham, WA, pp. 205–216.

Kramer, H. P. & Bruckner, J. B. (1975), 'Iterations of a non-linear transformation for enhancement of digital images', *Pattern recognition* **7**, 53–58.

Levin, D. N., Pelizzari, C. A., Chen, G. T. Y., Chen, C. & Cooper, M. D. (1988), 'Retrospective geometric correlation of MR, CT, and PET images', *Radiology* **169**(3), 817–823.

Maes, F., Collignon, A., Vandermeulen, D., Marchal, G. & Suetens, P. (1996*a*), Multi-modality image registration by maximization of mutual information, *in* 'Mathematical methods in biomedical image analysis', IEEE computer society press, Los Alamitos, CA, pp. 14–22.

Maes, F., Collignon, A., Vandermeulen, D., Marchal, G. & Suetens, P. (1996*b*), 'Multi-modality image registration by maximization of mutual information', *IEEE Transactions on medical imaging* . In press.

Maintz, J. B. A., van den Elsen, P. A. & Viergever, M. A. (1994), Using geometrical features to match CT and MR brain images, *in* L. Beolchi & M. Kuhn, eds, 'Medical imaging, analysis of multimodality 2D/3D images', Vol. 19 of *Studies in Health, Technology and Informatics*, IOS Press, Amsterdam, pp. 43–52.

Maintz, J. B. A., van den Elsen, P. A. & Viergever, M. A. (1995), Comparison of feature-based matching of CT and MR brain images, *in* N. Ayache, ed., 'Computer vision, virtual reality, and robotics in medicine', Vol. 905 of *Lecture notes in computer science*, Springer-Verlag, Berlin, pp. 219–228.

Maintz, J. B. A., van den Elsen, P. A. & Viergever, M. A. (1996), 'Evaluation of ridge seeking operators for multimodality medical image matching', *IEEE Transactions on pattern analysis and machine intelligence* **18**(4), 353–365.

Maintz, J. B. A., van den Elsen, P. A. & Viergever, M. A. (1997), 'Comparison of edge-based and ridge-based registration of CT and MR brain images', *Medical image analysis* **1**(2), 151–161. in press.

Pelizzari, C. A., Chen, G. T. Y., Spelbring, D. R., Weichselbaum, R. R. & Chen, C. T. (1989), 'Accurate three-dimensional registration of CT, PET, and/or MR images of the brain', *Computer assisted tomography* **13**(1), 20–26.

Schad, L. R., Boesecke, R., Schlegel, W., Hartmann, G. H., Sturm, G. H., Strauss, L. G. & Lorenz, W. (1987), 'Three dimensional image correlation of CT, MR, and PET studies in radiotherapy treatment of brain tumors', *Computer assisted tomography* **11**, 948–954.

Serra, J. (1982), *Image analysis and mathematical morphology*, Academic press.

Serra, J. (1988), *Image analysis and mathematical morphology, volume 2: theoretical advances*, Academic press.

Studholme, C., Hill, D. L. G. & Hawkes, D. J. (1995), Multi resolution voxel similarity measures for MR-PET registration, *in* Y. Bizais & C. Barillot, eds, 'Information Processing in Medical Imaging', Kluwer Academic Publishers, Dordrecht, pp. 287–298.

Taylor, R. H., Lavallée, S., Burdea, G. C. & Mösges, R. (1996), *Computer-integrated surgery*, Technology and clinical applications, MIT Press, Cambridge, MA.

van den Elsen, P. A., Maintz, J. B. A., Pol, E. & Viergever, M. A. (1995), 'Automatic registration of CT and MR brain images using correlation of geometrical features', *IEEE Transactions on medical images* **14**(2), 384–398.

van den Elsen, P. A., Pol, E. J. D. & Viergever, M. A. (1993), 'Medical image matching– a review with classification', *IEEE Engineering in medicine and biology* **12**(1), 26–39.

van den Elsen, P. A. & Viergever, M. A. (1994), 'Marker guided multimodality matching of the brain', *European radiology* **4**, 45–51.

van den Elsen, P. A., Viergever, M. A., van Huffelen, A. C., van der Meij, W. & Wieneke, G. H. (1991), 'Accurate matching of electromagnetic dipole data with CT and MR images', *Brain topography* **3**(4), 425–432.

Vandermeulen, D. (1991), Methods for registration, interpolation and interpretation of three-dimensional medical image data for use in 3-D display, 3-D modelling and therapy planning, PhD thesis, University of Leuven, Belgium.

Viergever, M. A., Maintz, J. B. A., Stokking, R., van den Elsen, P. A. & Zuiderveld, K. J. (1995), Matching and integrated display of brain images from multiple modalities, *in* 'Medical Imaging', Vol. 2434, SPIE Press, Bellingham, WA, pp. 2–13.

Viola, P. & Wells III, W. (1995), Alignment by maximization of mutual information, *in* 'International conference on computer vision', IEEE computer society press, Los Alamitos, CA, pp. 16–23.

West et al., J. (1996), Comparison and evaluation of retrospective intermodality image registration techniques, *in* M. H. Loew & K. M. Hanson, eds, 'SPIE proc MI', Vol. 2710, pp. 332–347.

Woods, R., Maziotta, J. & Cherry, S. (1993), 'MRI-PET registration with automated algorithm', *journal of computer assisted tomography* **17**(4), 536–546.